Received: 5 April 2019 | Revised: 17 June 2019 | Accepted: 17 June 2019

DOI: 10.1111/jace.16664

ORIGINAL ARTICLE

Journal of the American Ceramic Society

# Residual stress effect on the fracture toughness of lithium disilicate glass-ceramics

**Mariana O. C. Villas-Boas**[1] | **Francisco C. Serbena**[2] | **Viviane O. Soares**[3] | **Ivan Mathias**[2] | **Edgar D. Zanotto**[1]

[1]Vitreous Materials Laboratory (LaMaV), Department of Materials Engineering (DEMa), Federal University of São Carlos (UFSCar), São Carlos, SP, Brazil

[2]Department of Physics, State University of Ponta Grossa (UEPG), Ponta Grossa, PR, Brazil

[3]Department of Sciences, State University of Maringá (UEM), Goioerê, PR, Brazil

**Correspondence**
Mariana O. C. Villas-Boas, Vitreous Materials Laboratory (LaMaV), Department of Materials Engineering (DEMa), Federal University of São Carlos (UFSCar), São Carlos, SP, Brazil.
Email: marianaoc@yahoo.com.br

**Funding information**
Fundação de Amparo à Pesquisa do Estado de São Paulo, Grant/Award Number: 2013/07793-6; Conselho Nacional de Desenvolvimento Científico e Tecnológico, Grant/Award Number: 142561/2010-0; Coordenação de Aperfeiçoamento de Pessoal de Nível Superior, Grant/Award Number: 001; Brazilian Synchrotron Light Laboratory (LNLS/CNPEM/Campinas), Grant/Award Number: XRD1-13534

**Abstract**

In glass-ceramics (GCs), on cooling from the crystallization temperature, internal residual stresses are generated due to the difference between the thermal expansion coefficient (TEC) of the crystal phase(s) and the residual glass. These stresses could degrade or promote their mechanical properties. In this work, we varied the magnitude of the residual stresses in lithium silicate GCs by designing their microstructures. The level of internal stresses was measured using (Synchrotron) X-ray diffraction. The effects of anisotropy of thermal expansion, crystal shape, and intensity of the residual stresses were analyzed and compared using theoretical models. We extended the Hsueh-Becher model to include the thermal expansion anisotropy of the orthorhombic lithium disilicate (LS2) crystals. We found that the average residual stresses within the LS2 crystals are compressive or null (−100 to ~0) and highly anisotropic. Most importantly, within the limits of this study, we found no evidence for the influence of (compressive or null) residual stresses on the fracture toughness of the studied GCs. Within the crystal size range from 1 to 5 μm, a highly crystallized volume fraction coupled to relatively large crystals (5 μm) of high elastic modulus improved the glass-ceramic fracture toughness. This result can guide the microstructural design of novel tough GCs.

**KEYWORDS**

dental, fracture toughness, glass-ceramic, residual stress

## 1 | INTRODUCTION

Glass-ceramics (GCs) are inorganic, nonmetallic materials prepared by controlled crystallization of glasses via different processing methods. They contain at least one type of functional crystalline phase and a residual glass. The crystallized volume fraction may vary from ppm to almost 100%.[1] They are generally much stronger than the precursor glass and are used in many domestic and high-tech applications, such as electrical insulators, hard drive substrates, telescope mirrors, cooktop plates, construction and architecture—as synthetic marble or granite, dental prostheses, or as bioactive materials to replace or regenerate human bones and teeth.[1–3]

The traditional technique used to produce GCs consists of melting and vitrification, forming a desired glass article of a certain shape, and subjecting it to thermal treatment to induce crystal nucleation and growth inside the piece. In this stage, it is very important to induce copious internal nucleation and crystallization to form a rigid backbone that precludes sagging and deformation of the article (that still contains a significant fraction of glass phase). Using this method, GCs with tight microstructural control can be obtained. They can

 © 2019 The American Ceramic Society 

be tailored to show well-defined crystal phases, variable crystal sizes and a degree of crystallization, which result in desirable properties.

Among many types of laboratory and commercial GCs, those containing lithium disilicate ($Li_2Si_2O_5$ = LS2) crystals stand out due to their successful use as dental prostheses. In this material, internal crystallization occurs easily, and the crystals are homogeneously dispersed in the glass sample interior; hence, they serve as models for the study of more complex GCs. For this reason, the crystallization behavior of LS2-based glasses has been the subject of many studies, and a significant amount of kinetic, mechanical and thermodynamic data are available in the literature.[4–11] Also, lithium disilicate glass does not require the addition of nucleating agents to promote nucleation. However, adding $P_2O_5$ and $ZrO_2$, for example, significantly increases the rate of crystal nucleation[6,12–15] in these glasses.

Commercial LS2 GCs have been used for many applications, including intensive use as dental materials[16,17] due to their unique combination of properties: excellent biocompatibility, color stability, chemical durability, a similar hardness to teeth (important to prevent wear of the opposing tooth), translucency, simulating a natural look, as well as very high fracture strength (>350 MPa), and adequate fracture toughness ($K_{IC}$ = 2.5-2.8 MPa·m$^{1/2}$). This impressive combination of properties results from the high-volume fraction (~70%) of elongated micron-sized LS2 crystals, and some minor phases, which form an interlocking network embedded into a residual glass. The development of novel GCs, particularly LS2 based GCs, has significantly helped to improve the quality of materials for dental prostheses.[16,17]

LS2 GCs have adequate translucency, and hardness similar to natural teeth. However, their relatively high, but still inferior mechanical strength (<400 MPa) when compared to Zirconia prostheses (~1000 MPa) [18], restrict their application to two or less element bridges.[16,17,19,20] Considering this, changes in the base glass composition and the microstructure design through suitable heat treatments, in principle, could enable the production of LS2 GCs to have superior fracture strength and toughness.[9]

The chemical composition of the base glass and crystallization heat treatments can be tailored to produce different crystal shapes and sizes and the percentage of crystalline phases to generate different levels (and type) of residual stresses. These may optimize the mechanical properties of GCs, allowing not only the expansion of the LS2 GCs application, but also for all other types of GCs that have similar microstructures.[9,21–24] Several aspects of the microstructure affect the mechanical properties of GCs and warrant a more in-depth investigation: the nature of the crystallized phases, the crystallized volume fraction, the crystal size and shape, and the level and type (compression or tension) of internal residual stresses. These will be focused on here. Some authors[4,11,21–24] reasonably stated that residual stresses could have an effect on the fracture toughness. These stresses may positively or negatively affect the GC´s mechanical performance, but this matter is far from clear. Therefore, the aim of this work is to determine the effect of residual stresses on the toughness of GCs.

Previously, we measured the residual stresses in *stoichiometric* LS2 GCs.[4,25] In those studies, the crystallized volume fractions were quite low (8%-10% in Ref. 4 and 4%-7% in Ref. 25), the LS2 crystals had an ellipsoidal shape with a 1.6:1 axis ratio, the residual stresses varied with crystallographic direction due to the thermal expansion anisotropy, and the average thermal stress in the crystals was compressive, in agreement with Selsing´s model. In this research, we significantly extend the previous investigations by using nonstoichiometric compositions, high crystallized volume fractions, lath-shaped crystals, vary the *magnitude* and *type* of the residual stresses and test their effect on the fracture toughness of the GCs. We also extended the model itself to include the effect of high crystalline volume fraction and thermal anisotropy, factors that are not taken into account by Selsing's model.

Four types of GCs were designed by varying key microstructural aspects to develop multiphase brittle materials having superior mechanical properties. We varied the chemical composition and thermal treatments to achieve lath-shaped crystals of a size below 5 μm; aiming to obtain GCs having *high* and *low* crystallized volume fractions. Moreover, and most demanding, we designed their compositions so the density of the residual glasses was close to that of the LS2 crystal. Furthermore, the compositions and resulting thermal expansion coefficients (TECs) of the residual glasses were designed to be *similar* or *higher* than the average TEC of the major crystal phase LS2 (~$10 \times 10^{-6}$ K$^{-1}$), allowing for the production of different levels and types of residual stresses. In the end, after trying 50 compositions and 200 thermal treatments, we were able to produce some GCs with almost null residual stress (−10 MPa) and others with significant compressive stresses (−100 MPa) within the LS2 crystals.

We hope that the design concepts advanced here and results of this article for LS2 may be used for developing other types of GCs, allowing optimization of their microstructures to obtain desired properties.

## 2 | EXPERIMENTAL PROCEDURE

The guidelines used to design the parent glass compositions were: (a) the sum of the $Li_2O$ and $SiO_2$ concentrations were kept constant at 80 wt% with the assumption that most $Li_2O$ would be uptaken by the growing crystals during crystallization, (b) the densities of the residual glasses should be similar to those of the LS2 crystal and, finally, the thermal expansion of the residual glasses ($\alpha_{rg}$) should be *similar* or *higher* to those of the (average) $LS_2$ crystal ($\alpha_{LS2} = 10.1 \times 10^{-6}$ K$^{-1}$).[4]

The compositional design constrain (b) is to minimize the possibility of formation of crystal phases that are much denser than the residual glass, which could trigger "cavitation" pores in the GC. The softwares Interglad[26] and SciGlass[27] were used to design (predict) the residual glass composition after crystallization to meet all these criteria.

More than 50 glass compositions and approximately 200 heat treatments were designed and tested to obtain the desired materials throughout a one-year preliminary (but fundamental) study. Among all these, two compositions and four heat treatments that satisfied the criteria of *high* and *average* TEC, lath-shaped crystals of less than 5 μm, and high and low crystallized volume fractions (*f*), were selected and are shown in Table 1. The chemical composition (mol%) of the parent glass for equal TEC was $SiO_2$ (65.36%), $Li_2O$ (26.64%), $P_2O_5$ (1.20%), $Sb_2O_3$ (0.60%), $K_2O$ (3.52%), MgO (1.28%), $Al_2O_3$ (1.08%), CaO (0.20%) and BaO (0.13%). For higher TEC it was $SiO_2$ (61.65%), $Li_2O$ (30.35%), $P_2O_5$ (2.10%), $Sb_2O_3$ (0.68%), $K_2O$ (3.50%), ZnO (0.15%) and $Na_2O$ (1.57%).

We also tried to design GCs having a residual glass with *lower* TEC than those of the LS2 phase. More than 15 different glass compositions and 60 heat treatments were carried out with no success due to the simultaneous crystallization of three different phases that affected the final residual glass compositions and their thermal expansion. Therefore, in this article we only deal with residual glasses having *equal and higher* TEC than the LS2 crystal.

The optimization process of the heat treatments will be detailed in Section 3.1.2. It involved differential scanning calorimetry (DSC) measurements of the parent glass to determine the glass transition temperature ($T_g$) and the crystallization peaks, then heat treatments for nucleation and crystal growth and optimization of the heat treatment times.

The heat treatments were based on the DSC traces of two selected glasses. To best control the number and size of the crystals, as well as the crystallized volume fractions, we performed double-stage heat treatments. The maximum crystal nucleation rates of these GCs occur at temperatures near $T_g$ and, therefore, this temperature was chosen for the nucleation treatments that will be detailed in Section 3.2. The crystallized phases were identified by X-ray diffraction (XRD) using a Rigaku Ultima IV diffractometer with Cu-$K_\alpha$ radiation. The $2\theta$-range was continuously scanned from 10° to 120° with a step size of 0.02° and a speed of 2°/min.

Two very successful commercial dental LS2 GCs, produced by Ivoclar Vivadent,[16,17] IPS e.max® CAD and IPS e.max® PRESS, were also studied and compared with our samples. Specimens of both materials were prepared according to the procedures recommended by Ivoclar using an EP5000-Ivoclar oven. The microstructural evolution for each heat treatment was also followed by scanning electron microscopy (SEM) using a Philips XL-30 microscope employing secondary and backscattered electrons for morphology and compositional analysis.

The crystallized volume fractions were determined using XRD. Alumina powder was mixed to powdered GC samples in a 1:1 proportion by weight. They were measured in the $\theta$-$\theta$ geometry using a Rigaku Ultima IV diffractometer and the $2\theta$-range was scanned from 10° to 120° with a step size of 0.02° in the $2\theta$-scale and a time step of 6 seconds. The volume fractions of each phase were determined using Rietveld refinement of the XRD patterns using the GSAS[28] and the EXPGUI[29] packages, where the amorphous contribution was considered as a part of the background. Using a known amount of alumina added to the powdered GC and its estimated weight fraction obtained using Rietveld refinement, a simple rule of mixture allowed for the calculation of the volume fraction of each phase and the amount of residual glass.

The hardness ($H$) and elastic modulus ($E$) were measured as a function of the contact depth by instrumented nanoindentation using a Nanoindenter XP and the Oliver and Pharr method[30] with a Berkovich diamond indenter. The maximum load was 400 mN with a peak hold time of 15 seconds. Each data point was calculated from the average of at least 17 indentations. Furthermore, the Vickers hardness ($H_V$) was measured and calculated using $H_V = 1.854P/d^2$, where $P$ is the load and $d$ is the diagonal impression. The load was 3 N. The indentation fracture toughness technique was used for a preliminary fast screening of all the samples that seemed to possess the best

**TABLE 1** Designed residual glass (rg), calculated TEC of the residual glass (assuming crystallization of LS2), residual glass components, and heat treatments

| | Sample | Calculated $\alpha_{rg}$ ($10^{-6}$ $K^{-1}$) | Expected components in the residual glass | Desired crystallized volume fraction | Selected heat treatment |
|---|---|---|---|---|---|
| $\alpha_{rg} \sim <\alpha_{LS2}>$ | EL | 11 | $Si_2O$-$P_2O_5$-$Sb_2O_3$-$K_2O$-MgO-CaO-BaO-$Al_2O_3$ | Low | 450°C-10 min/840°C-10 min |
| | EH | | | High | 450°C-12 h/840°C-2 h |
| $\alpha_{rg} > <\alpha_{LS2}>$ | HL | 19 | $SiO_2$-$P_2O_5$-$Sb_2O_3$-$K_2O$-ZnO-$Na_2O$ | Low | 466°C-5 min/700°C-5 min |
| | HH | | | High | 466°C-15 min/589°C-15 min/805°C-2 h |

Abbreviation: TEC, thermal expansion coefficient.

toughness. The indentation fracture toughness ($K_C$) was calculated from the radial crack length ($c$) measurement produced by a Vickers indentation in air with a load of 3 N. The number of indentations per sample was 5. $K_C$ was calculated according to the Niihara equation[31]:

$$K_C = 0.035 \left(\frac{l}{b}\right)^{-1/2} \left(\frac{H_V}{E\phi}\right)^{-2/5} \left(\frac{H_V\sqrt{b}}{\phi}\right), \quad (1)$$

where $H_V$ is the Vickers hardness, $b$ is the half-impression diagonal, $l$ is the difference between the radial crack length and the half-impression diagonal and $\phi = 3$. The authors are well aware of the limitations of this technique,[32] however the indentation method is simple, easy and nondestructive. We believe it is capable of revealing semi-quantitative trends when comparing the same material with different microstructures, such as those of this study.

It is known that crystallization of glasses normally increases their fracture toughness.[33] The fracture toughness of GCs with the highest crystallized volume fractions was measured using the double torsion technique.[33–36] Notched specimens measuring 15 × 5 × 1 mm$^3$ were submitted for double torsion experiments using a special design jig in a universal testing machine (Shimadzu AGS-X 5 kN). The tests were performed in similar conditions as those detailed in ref.[33] The fracture toughness measured by double torsion ($K_{DTIC}$) was calculated as $P_C W_m \sqrt{3/Wt^4\,(1-\nu)\,\psi}$, where $W_m$ is the moment arm, $\nu$ is Poisson's ratio, $P_C$ is the load at fracture, and $\psi = 1 - 0.6302\,\tau + 1.20\,\tau\,\exp(-\pi/\tau)$, where $\tau = 2t/W$. The reported values refer to the average of five fractured samples.

The TECs of the different crystallized phases were measured in situ using high temperature XRD. The measurements were performed using the $\theta$-$\theta$ geometry and an Anton Paar heating stage coupled to a Rigaku Ultima IV diffractometer. The diffractograms were recorded using powdered samples of high crystallized volume fractions, in the $2\theta$ range from 10° to 70°, in 0.020° or 0.025° steps at 40, 160, 280 and 400°C using Cu-Kα radiation and time steps of 12 or 20 seconds. A Rietveld refinement of the diffractograms recorded at each temperature was carried out using the GSAS and the EXPGUI packages to determine the lattice parameter variations with temperature.

The thermal expansion of the parent glass and the highly crystallized GCs ($\alpha_{gc.exp}$) were measured using dilatometry using a heating rate of 5 K·min$^{-1}$ in air, up to 400°C. Cylindrical shaped samples, 35 mm long, were prepared by cutting and polishing to obtain parallel faces. The experimental TEC of the residual glass ($\alpha_{res.glass}$) was estimated using a rule of mixture:

$$\alpha_{res.glass} = \frac{\alpha_{gc.exp} - f.\bar{\alpha}_{cryst.vol}}{1-f}, \quad (2)$$

where $\bar{\alpha}_{cryst.vol}$ is the average thermal expansion of all crystallized phases, estimated from the thermal expansion measurements and the crystallized volume fractions measured using XRD. From the measurements of the crystallized volume fraction of each phase, the chemical composition of the residual glass for each GC was estimated and its TEC was calculated using the SciGlass software.

The residual stresses were measured by XRD using synchrotron radiation at the XRD2 beamline of the Brazilian National Synchrotron Light Laboratory. Samples in bulk and powder forms were measured. Stress-free reference samples for each composition and thermal treatment were prepared by crushing bulk samples using an agate pistil and mortar and sieving it through a 22 μm mesh. Therefore, the maximum particle size was 22 μm, with a typical size distribution between 1 and 20 μm, ie, a similar distribution as the LS2 crystals. Also, the surfaces of the powder particles were micro-cracked during the crushing procedure, which relieved the residual stresses. All monolithic specimens were annealed at 20°C below $T_g$ for 2 hours followed by slow cooling to room temperature to relieve any macroscopic stresses that were eventually induced during sample preparation for mechanical testing.

The diffractograms were performed in the $\theta$-$2\theta$ geometry at room temperature using a (002) highly oriented pyrolitic graphite analyzer. The wavelength was set to 1.549370(2) Å, calibrated against a $LaB_6$ standard NIST-660a. The $2\theta$-range was scanned from 5° to 70° and the step size amounted to 0.01° or 0.02° in the $2\theta$-scale. The samples were rotated during the measurements to minimize the possible effect of texture or poor grain statistics. The lattice parameters of the bulk and powder GC samples were refined using the GSAS and the EXPGUI package. The lattice strains of the LS2 crystalline phase were evaluated for each GC sample assuming the corresponding powdered sample as a stress-free reference.

The strain $\varepsilon_i$ along each crystallographic direction was calculated as:

$$\varepsilon_i = \frac{\Delta a^i}{a_0^i} \quad (3)$$

where $\Delta a^i$ is the difference between the lattice parameters of the strained (bulk) and the stress-free (powder) samples along that specific crystallographic direction.

The average residual stress ($\bar{\sigma}$) was then calculated using Hooke's law and assuming a hydrostatic triaxial stress state of the crystals:

$$\bar{\sigma} = \frac{E_p}{1-2\nu_p}\bar{\varepsilon}, \quad (4)$$

where $E_p$ is the average elastic modulus and $\nu_p$ is the Poisson ratio of the LS2 crystal phase, and $\bar{\varepsilon} = \sum_i \varepsilon_i / 3$.

# 3 | RESULTS

## 3.1 | Microstructures

### 3.1.1 | IPS e.max® CAD and IPS e.max® PRESS GCs

The microstructures of the IPS e.max® CAD and IPS e.max® PRESS samples, after the manufacturer's recommended heat treatment in an EP5000 oven, indeed showed high crystallized fractions (54 and 78%, respectively), elongated crystals of an average size of 5 × 1 μm, as shown in Figure 1. In the IPS e.max® PRESS, the crystals were slightly oriented due to the injection step, which can be expected owing to the high aspect ratio of these crystals.

The XRD patterns of the IPS e.max® CAD and IPS e.max® PRESS samples are shown in Figure 2. The presence of LS2 and $Li_3PO_4$ crystal phases were detected. The IPS e.max® CAD presented 46% of residual glass; higher than the IPS e.max® PRESS with 22%, as indicated in Table 2. The amount of the LS2 phase was 49% for the CAD and 68% for the PRESS. $Li_3PO_4$ also appeared with 5% and 10% volume fractions for CAD and PRESS, respectively. In both GCs, a very small amount of quartz was also detected. The specialized literature indicates a crystallized volume fraction of 70% of the LS2 phase for IPS e.max® CAD[37] and 65% for IPS e.max® PRESS.[38]

### 3.1.2 | Designed GCs

In order to investigate the effect of residual stresses on the mechanical properties of LS2 GCs, we formulated different glass-forming compositions aiming at achieving different types of residual glasses (after crystallization) to have *higher* and *similar* TEC than the average value of the LS2 crystal. Therefore, the type of residual stresses on the crystals would vary from compressive to null.

We also studied the effect of the crystallized volume fraction. Our GCs were designed to have 80% vol. crystallized of LS2 and 20% vol. of residual glass, and also a low crystallized fraction for each condition of TEC of the residual glass. The compositional design was not perfect because we assumed that the only phase present after crystallization would be the stoichiometric LS2. In the end, this was not the case as other phases crystallized. However, after some experimentation, we indeed reached the desired cases of medium and high TEC.

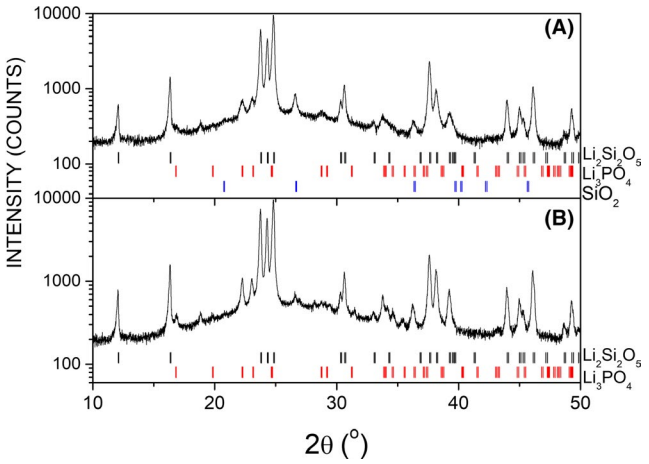


**FIGURE 2** X-ray diffractograms of crystallized (A) IPS e.max® CAD and (B) IPS e.max® PRESS GCs. The peak positions of $Li_2Si_2O_5$ (black), $Li_3PO_4$ (red) and $SiO_2$ (blue) phases are marked. GCs, glass-ceramics

**TABLE 2** Crystallized volume fractions of the IPS e.max® CAD and IPS e.max® PRESS GCs (treated in a dental technician furnace) calculated using Rietveld refinement

| | $Li_2Si_2O_5$ (%) | $Li_3PO_4$ (%) | Residual glass (%) |
|---|---|---|---|
| CAD | 49 | 5 | 46 |
| PRESS | 68 | 10 | 22 |

Abbreviation: GCs, glass-ceramics.

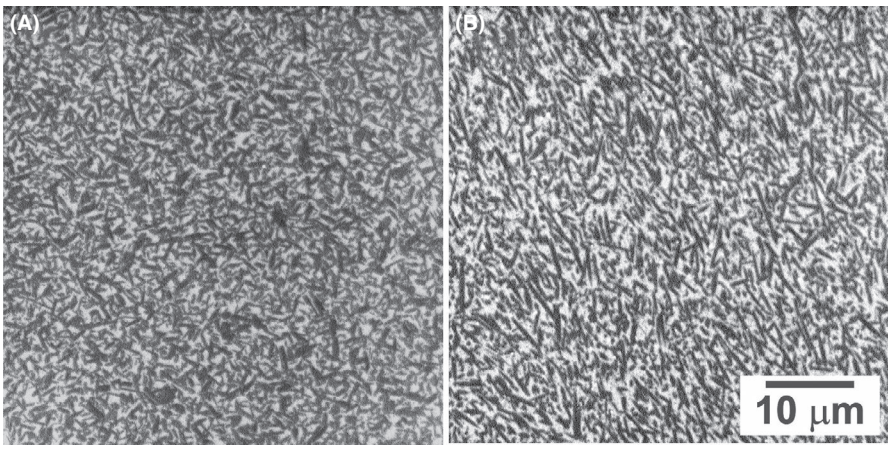


**FIGURE 1** Backscattered SEM images of commercial dental GCs. (A) IPS e.max® CAD and (B) IPS e.max® PRESS. GCs, glass-ceramics; SEM, scanning electron microscopy

*TEC of the residual glass similar to the LS2 crystal phase*

To obtain a GC containing a residual glass having a TEC similar to the LS2 crystal phase, we designed a composition having $SiO_2$, $Li_2O$, $P_2O_5$, $Sb_2O_3$, $K_2O$, MgO, CaO, BaO and $Al_2O_3$ so the residual glass (after crystallization) should have a TEC of $11 \times 10^{-6}\ K^{-1}$. The DSC of the obtained glass, Figure 3, shows that its $T_g$ is 450°C, and it shows a single crystallization peak.

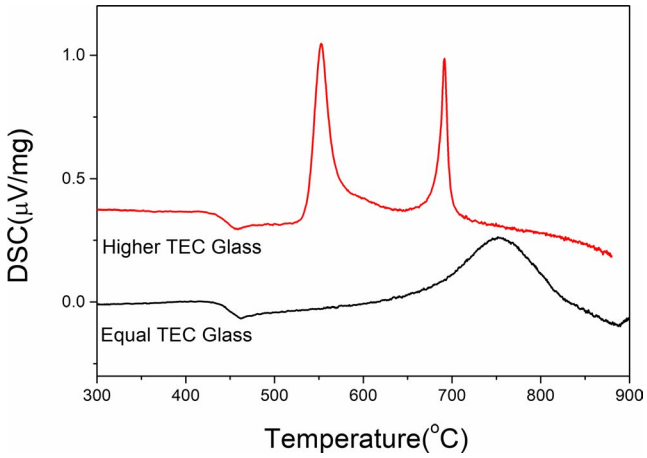


**FIGURE 3** DSC of the glasses designed to have residual vitreous phases with TEC equal and higher than the LS2 crystalline phase. TEC, thermal expansion coefficient

The growth treatment was performed at 840°C, at the end of the crystallization peak. Samples were heat treated at 450°C at different times for nucleation (10 minutes, 30 minutes, 3 hours and 12 hours) and at 840°C for growth (10 minutes, 1 hour and 2 hours). Analyses of the resulting microstructures using SEM showed, as expected, that as the nucleation time increases (10 minutes-12 hours), the crystals decrease in size and increase in quantity. Regarding the growth time, the microstructure of the samples treated for 3 hours for nucleation and for 1 and 2 hours for crystal growth were similar.

Therefore, the chosen heat treatments were at 450°C/10 min and 840°C/10 min for the low crystallized fraction (EL), and 450°C/12 h and 840°C/2 h for the high crystallized volume fraction (EH). The microstructures of these samples are shown in Figure 4A,B, respectively. Figure 4A shows lath-shaped crystals larger than 5 μm. The more or less round crystals may be the cross section of the laths. Figure 4B shows crystals of approximately 5 μm.

*TEC of the residual glass higher than the LS2 crystal phase*

For the residual glass having a TEC *higher* than the average of the LS2 crystal, a composition with $SiO_2$, $Li_2O$, $P_2O_5$, $Sb_2O_3$, $K_2O$, ZnO and $Na_2O$ was designed with the aim of a achieving a residual glass TEC of $19 \times 10^{-6}\ K^{-1}$. The DSC

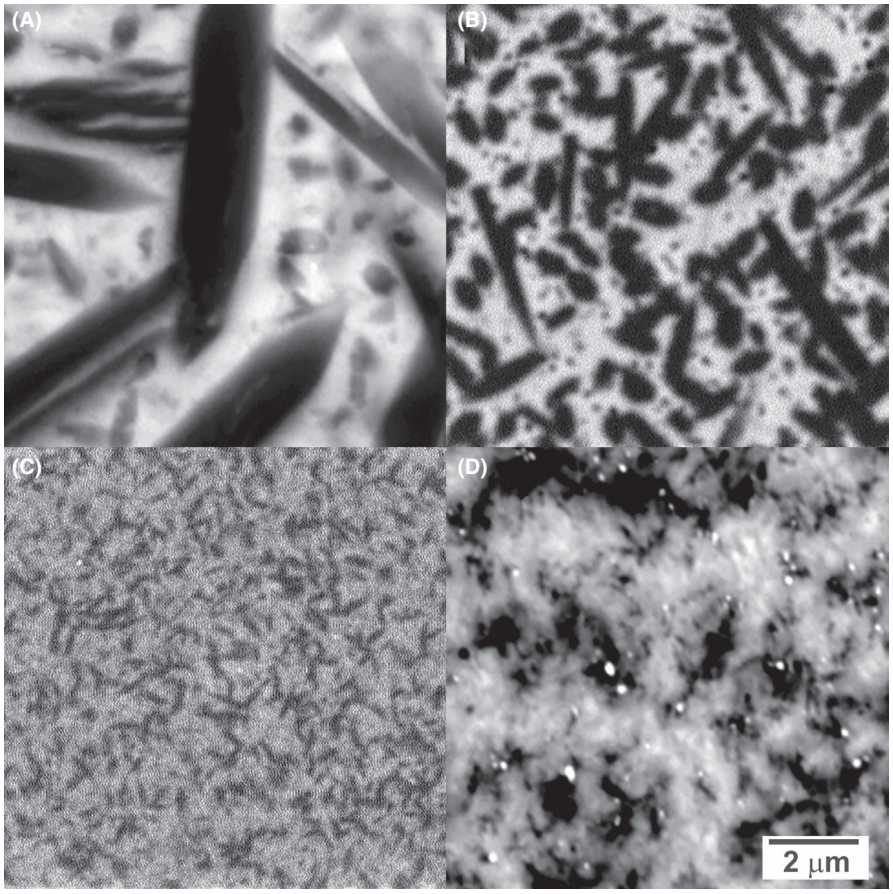


**FIGURE 4** Backscattered SEM revealing the microstructures of (A) EL, (B) EH, (C) HL and (D) HH glass-ceramics. SEM, scanning electron microscopy

showed that the $T_g$ of the parent glass was 433°C, and two very intense and separated crystallization peaks were present at 560°C and 705°C, as shown in Figure 3. To identify the two phases related to these two peaks, a triple heat treatment was performed, where the sample was nucleated at $T_g$. Two additional heat treatments for crystal growth were performed after the first crystallization peak at 589°C, and then after the second peak at 805°C. With this triple heat treatment, two phases were obtained: lithium metasilicate ($Li_2SiO_3$ = LS) and LS2.

A GC presenting some LS, which is a highly machinable phase, is important and desired because of the possibility of producing monolithic pieces using the CAD/CAM technique. The LS crystals have much higher machinability than the LS2 and the vitreous phase.[39] Regarding its microstructures, we observed that the crystals were not within the aimed 2.5-5.0 μm range size. Thus, a new sample was nucleated at 466°C (33°C above $T_g$), to decrease the nucleation rate and the time was reduced to 8 minutes. The heat treatments for crystal growth were at the same temperatures and the size of the crystals increased slightly. With the help of XRD measurements, the heat treatments chosen were 466°C/5 min and 700°C/5 min for the low crystalline volume fraction (HL), and 466°C/15 min, 589°C/15 min and 805°C/2 h for the high crystalline volume fraction (HH).

The final microstructures are shown in Figure 4C,D. They are indeed close to the expected microstructures, with lath-shaped crystals of approximately 1 μm. The bright dots observed in Figure 4C refer to (not assumed in the compositional design) $Li_3PO_4$.

## 3.2 | Crystallized phases

Figure 5 shows the XRD diffractograms for the final GCs. The main crystal phase in all samples is LS2. However, $Li_2SiO_3$ and $Li_3PO_4$ diffraction peaks can also be observed.

The phase quantification is shown in Table 3. The main crystal phase is $Li_2Si_2O_5$. $Li_3PO_4$ is also present in small concentration in all samples. Finally, from 3% to 12% of the $Li_2SiO_3$ phase is also present in samples HL and HH. Sample EL had a crystallized volume fraction of 22%. For samples EH, HL and HH, there is no large difference between the crystallized volume fractions, as all of them were in the range of 41%-48%.

## 3.3 | Mechanical properties

Vickers hardness ($H_V$) data presented in Table 4 show that the highest $H_V$ were those of the HL and HH samples probably due to the higher percentage of crystallized phases. The EL sample has the lowest $H_V$. This is probably caused by the greatest concentration of the LS phase. The $H_V$ of the samples EH, HL and HH were close to the $H_V$ of the commercial materials, as shown by Tables 4 and 5.

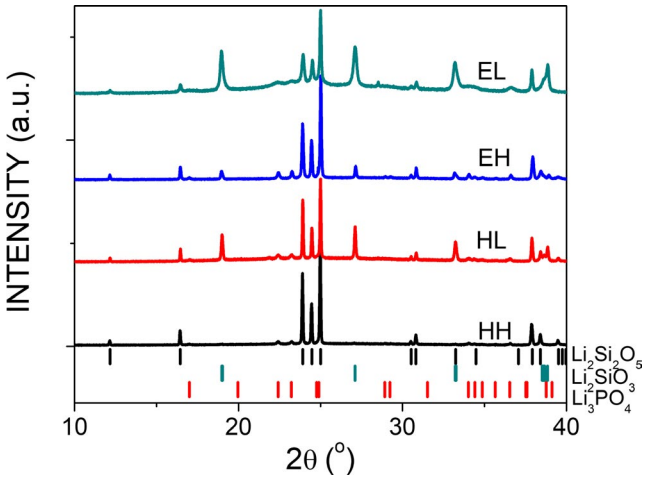


**FIGURE 5** X-ray diffractograms using synchrotron radiation of crystallized phases of EL, EH, HL and HH GCs. Peak positions of $Li_2Si_2O_5$ (black), $Li_2SiO_3$ (green) and $Li_3PO_4$ (red) phases are marked. GCs, glass-ceramics

**TABLE 3** Crystallized volume fractions of the two designed LS2 glass-ceramics (Rietveld analysis)

| Glass-ceramic | $Li_2Si_2O_5$ (%) | $Li_3PO_4$ (%) | $Li_2SiO_3$ (%) | Residual glass volume fraction |
|---|---|---|---|---|
| EL | 7 | 3 | 12 | 78 |
| EH | 38 | 3 | — | 59 |
| HL | 37 | 8 | 3 | 52 |
| HH | 33 | 7 | 7 | 53 |

The variation of $H_V$ and elastic modulus ($E$) as a function of the contact depth is shown in Figure 6. The values of $H_V$ measured by nanoindentation using a Berkovich indenter were larger, but followed the same trend observed by the Vickers hardness measurements.

**TABLE 4** Vickers hardness ($H_V$), hardness by instrumented indentation (H), elastic modulus ($E$), indentation fracture toughness ($K_C$) and double torsion toughness ($K_{DTIC}$) of the designed glass-ceramics. The numbers in brackets are the standard deviations corresponding to the last significant digit

| | $H_V$ (GPa) | H (GPa) | $E$ (GPa) | $K_C$ (MPa·m$^{1/2}$) | $K_{DTIC}$ (MPa·m$^{1/2}$) |
|---|---|---|---|---|---|
| EL | 5.25 (1) | 6.8 (2) | 95 (2) | 1.40 (5) | — |
| EH | 5.71 (1) | 6.6 (1) | 98 (2) | 1.52 (5) | 2.2 (1) |
| HL | 6.12 (1) | 7.3 (1) | 96 (1) | 1.25 (3) | — |
| HH | 5.71 (1) | 7.3 (1) | 107 (1) | 1.73 (6) | 2.0 (1) |

**TABLE 5** Mechanical properties of the IPS e.max® CAD and IPS e.max® PRESS glass-ceramics

| | $H_V$ (GPa) | $E$ (GPa) | $K_C$ (MPa·m$^{1/2}$) | $K_{IC}$ (MPa·m$^{1/2}$)[a] |
|---|---|---|---|---|
| CAD | 5.81 (1) | 95 | 1.62 (2) | 2.25 |
| PRESS | 5.78 (1) | 95 | 1.69 (3) | 2.75 |

[a]Ivoclar catalog.

The elastic moduli were equal to or higher than those of the commercial materials (Tables 4 and 5, respectively). The highest value was obtained for the HH sample. The data in Table 3 show that the EH sample has the highest amount of LS2. A high $E$ contributes to good mechanical performance.

The $K_C$ is shown in Table 4. Figure 7 shows a Vickers indentation with four such cracks radiating from the impression corners, as an example of the measured micrographs used to obtain $K_C$. All GCs have a value in the range of 1.0-1.7 MPa·m$^{1/2}$. The GCs with the higher crystallized volume fractions had a higher value of $K_C$ than those with a lower crystallized volume fraction. Sample HH had a $K_C$ value close to or higher than the commercial GCs IPS e.max® CAD and IPS e.max® PRESS reported in Table 5.

Therefore, we decided to measure the fracture toughness using the double torsion technique ($K_{DTIC}$) in the designed GCs having the highest crystallized volume fractions. Table 4 shows that the values are in the range of 2.0-2.2 MPa·m$^{1/2}$, close to the value of 2.25 MPa·m$^{1/2}$ reported for the IPS e.max® CAD,[40] GC and 20% below the IPS e.max® PRESS, as shown in Table 5.

## 3.4 | Thermal expansion

The use of high temperature XRD allowed for the determination of the TECs of the crystalline phases. One advantage of using this technique is that it measures the thermal expansion anisotropy for each crystal phase. The results for the thermal dilation of each direction of the unit cell as a function temperature for each phase observed in the GCs are displayed in Figure 8A-C for LS2, $Li_3PO_4$ and LS phases, respectively.

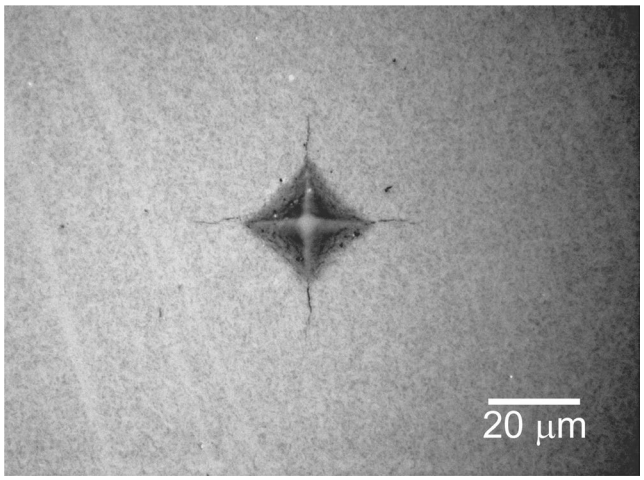


**FIGURE 7** Photo of a 3N Vickers indentation with cracks in the HH glass-ceramic

The thermal expansion is very anisotropic for all phases. For example, it varies from $6.5 \times 10^{-6}$ K$^{-1}$ to $13.3 \times 10^{-6}$ K$^{-1}$ for LS2, and from $9 \times 10^{-6}$ K$^{-1}$ to $22 \times 10^{-6}$ K$^{-1}$ for LS (Figure 8A,C, respectively). The calculated average linear TECs for each phase are shown in Table 6. The average TEC of $10.4 \times 10^{-6}$ K$^{-1}$ measured using high temperature XRD of the LS2 phase is in agreement with the value of $10.8 \times 10^{-6}$ K$^{-1}$ reported by Mastelaro and Zanotto.[4] The average value measured for the LS phase in this study is 15% lower than $18.1 \times 10^{-6}$ K$^{-1}$ measured by Richet et al[41] in the temperature range 20°C-400°C. Moreover, the TECs in this study were 22, 15 and $9 \times 10^{-6}$ K$^{-1}$ for the a, b and c axis, respectively. The measured values by Richet et al were 23.7, 23.0 and $7.6 \times 10^{-6}$ K$^{-1}$ for the a, b and c axis, respectively, in fair agreement with our study.

These values of TECs of each phase enable us to calculate the thermal expansion of the *residual glass*. Table 7 shows the TECs calculated by SciGlass from their nominal compositions and the experimentally measured value of the parent glasses. The agreement is very good.

Table 7 also reports on the experimental TEC of the GCs and the average TEC of the crystalline phases (not including the residual glass) calculated using the rule of mixture—from

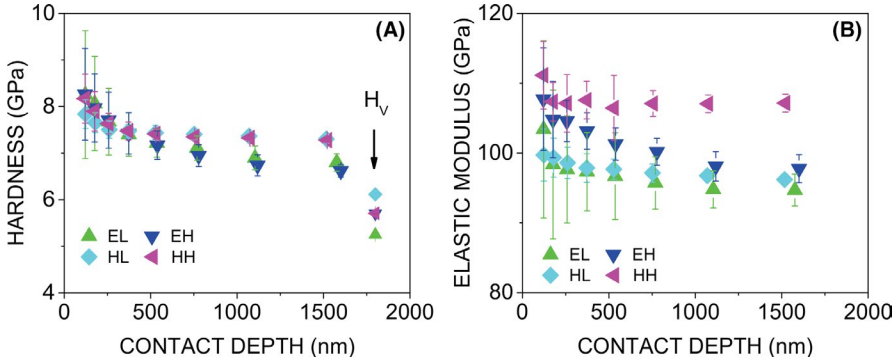


**FIGURE 6** (A) Hardness and (B) elastic modulus variation with a contact depth for the different glass-ceramics measured using instrumented indentation. Hardness measured using Vickers indentation ($H_V$) is also plotted in (A)

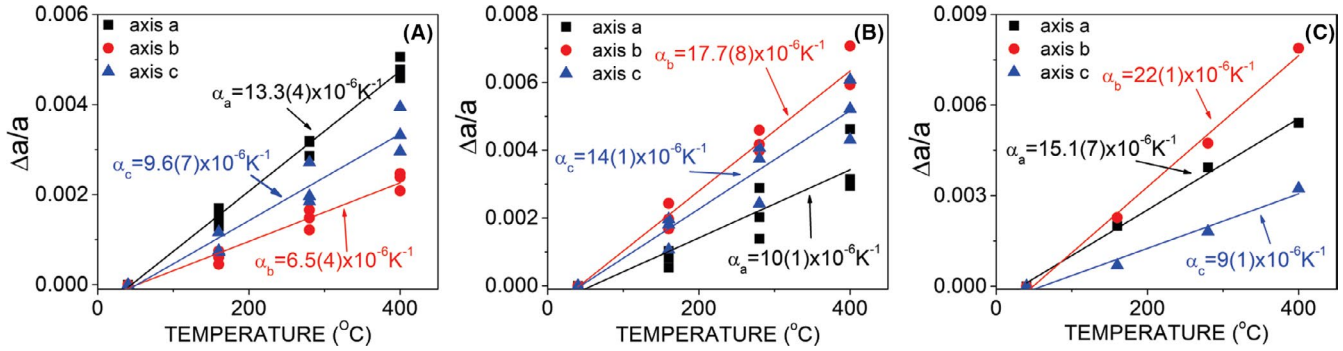


**FIGURE 8** Thermal expansion anisotropy measured using high temperature XRD of (A) $Li_2Si_2O_5$, (B) $Li_3PO_4$ and (C) $Li_2SiO_3$ crystal phases

the crystallized volume fraction and TEC measured using XRD for each phase. The correct trend can be observed regarding the designed type of stress (null or compressive) in the LS2 crystals. The sample EH has a TEC of the residual glass very close to LS2, which is a necessary condition to obtain a glass-ceramic with null residual stress, whereas the HH sample has a residual glass with a TEC higher than LS2, therefore compressive stresses are expected in the crystalline phases, as originally intended and designed. From the volume fraction of each crystalline phase and the amount of residual glass reported in Table 3, we estimated the chemical composition of the residual glasses, as shown in the Table 8. By using the SciGlass software, we then calculated the TEC of the residual glasses. There is very good agreement between the values predicted by SciGlass and the calculated values using Equation (2) for EH and HH samples.

These data also enabled us to estimate the TEC of the GCs with all crystallized crystal phases and the residual glass of the commercial IPS e.max® PRESS and IPS e.max® CAD GCs. The values are reported in Table 7.

### 3.5 | Residual stresses

The strain along each direction of the $Li_2Si_2O_5$ unit cell and the average residual stresses measured using XRD are shown in Table 9. Strain anisotropy is observed for all samples. The magnitude varies with crystallographic direction and depends on the TECs of the residual glass and the other phases; it could be positive or negative. In this case, the residual stresses calculated using Equation (4) are *compressive*, in which they are largest for the EL samples (−102 MPa), and in the range −12 to −49 MPa for the other samples. For the calculations, we assumed $E_p$ = 133 GPa and $\nu_p$ = 0.19.[4] The average residual stresses for the IPS e.max® CAD and IPS e.max® PRESS are also slightly *compressive*; −28 and −43 MPa, respectively.

**TABLE 6** Average linear thermal expansion coefficients of the different phases crystallized in the current glass-ceramics as measured using high temperature XRD in the temperature range 40°C-400°C

| Crystalline Phase | $\bar{\alpha}$ ($10^{-6}$ $K^{-1}$) |
|---|---|
| $Li_2Si_2O_5$ | 10.4 (3) |
| $Li_3PO_4$ | 14.1 (6) |
| $Li_2SiO_3$ | 15.4 (5) |

## 4 | DISCUSSION

The residual stresses in the LS2 crystals were compressive in all samples, varying from −12 ± 8 MPa (almost null) to −102 ± 9 MPa (compressive). The simplest model to predict residual thermal stresses is Selsing's.[42,43] It considers a single spherical precipitate embedded in an infinite matrix, where the precipitate and the matrix are isotropic and homogeneous. The residual stresses in the precipitate are given by:

$$\sigma_P = \frac{\Delta\alpha.\Delta T}{K_E} \quad (5)$$

where $\Delta\alpha$ is the linear thermal expansion difference between the precipitate (p) and the glass matrix (m), $\Delta T$ is the difference between $T_g$ and room temperature, $K_E = (1+\nu_m)/2E_m + (1-2\nu_p)/E_p$ and $\nu$ is Poisson's ratio. Taking $T_g$ = 455°C, $\alpha_m = 12.2\times10^{-6}\,K^{-1}$, $\alpha_p = 10.1\times10^{-6}\,K^{-1}$, $\nu_m$ = 0.215, $\nu_p$ = 0.19, $E_m$ = 80 GPa and $E_p$ = 133 GPa,[4] a stress of −74 MPa (compressive) is predicted. This value is well within the measured range.

Although Selsing's model gives a preliminary idea about residual stresses in GCs, it is only valid for low crystallized volume fractions of isotropic particles. However, as observed in Figures 1 and 4, the LS2 crystals have a lath shape, and high temperature XRD experiments revealed a significant TEC anisotropy of all crystal phases. Therefore, a more realistic model of the residual stress must be considered, which takes into account the thermal expansion anisotropy, precipitate shape, and the crystallized volume fraction. Selsing's model does not consider any of these factors.

**TABLE 7** Measured and calculated thermal expansion of the base glass, glass-ceramics, crystallized volume, and residual glass for the high-volume fraction glass-ceramics

| Phase | Method of calculation | Thermal expansion ($10^{-6}$ $K^{-1}$) | | | |
|---|---|---|---|---|---|
| | | EH | HH | CAD | PRESS |
| Parent glass | Calculated via SciGlass | 11.4 | 13.4 | — | — |
| | Experimental | 11.8 | 14.1 | — | — |
| Glass-ceramic | Experimental | 10.4 | 12.3 | 10.7 | 10.9 |
| Average TEC of crystallized phases ($\alpha_{cryst.vol}$) | Rule of mixture* | 10.7 | 11.7 | 11.1 | 10.9 |
| Residual glass | From experimental data** | 10.2 | 12.8 | 10.1 | 9.4 |
| | Calculated via SciGlass*** | 10.5 | 12.1 | — | — |

Abbreviation: TEC, thermal expansion coefficient.
*From high temperature X-ray diffraction.
**Using Equation (2).
***See residual glass composition in Table 8.

One model that considers all these effects was advanced by Hsueh and Becher (H-B).[44,45] Their model was developed for composites with fillers having *hexagonal* crystalline structure, such as SiC and graphite. Therefore, it considers only thermal anisotropy with two components along the *a* and *c* crystallographic directions of the hexagonal unit cell. As our main crystalline phase is $Li_2S_2O_5$ and has an orthorhombic unit cell, it has three components of the thermal expansion, as measured in Figure 8A, and Hsueh and Becher's model cannot be directly applied to our experiments.

We, therefore, *extended the H-B model* by considering an ellipsoidal precipitate (an approximation of the actual lath crystal shape) with three different TECs ($\alpha_a$, $\alpha_b$ and $\alpha_c$) embedded in an isotropic matrix, with a crystallized volume fraction (*f*), as in Figure 9. Both the precipitate and the matrix are elastically isotropic.

As the thermal expansion of the precipitate is different from the matrix, there will be three "transformations strains" $\varepsilon_{ii}^{t*} = (\alpha_i - \alpha_m)\,\Delta T$ along each crystallographic direction. These strains induce "constrained strains" $\varepsilon_{ij}^{c}$ in the inclusion given as $\varepsilon_{ij}^{c} = S_{ijkl}\varepsilon_{ij}^{t} + \varepsilon_{ij}^{c''}$, where $S_{ijkl}$ is the Eshelby's tensor,[45] $\varepsilon_{ij}^{t}$ is the "equivalent transformation strain" and $\varepsilon_{ij}^{t}$ is the average elastic strain in the matrix. The force equilibrium condition requires that $(1-f)\,\varepsilon_{ij}^{c''} + f\left(\varepsilon_{ij}^{c} - \varepsilon_{ij}^{t}\right) = 0$. The combination of these equations for our system results in:

$$\varepsilon_{ii}^{c} = (1-f)\sum_{j=1}^{3} S_{iijj}\varepsilon_{jj}^{t} + f\varepsilon_{ii}^{t} \tag{6}$$

Moreover, the equivalence between the true inclusion and the "equivalent inclusion" leads to[44,46]:

$$\begin{aligned} &2\mu_P\left(\varepsilon_{ii}^{c} - \varepsilon_{ii}^{t*}\right) + \lambda_P\sum_{j=1}^{3}\left(\varepsilon_{jj}^{c} - \varepsilon_{jj}^{t*}\right) \\ &= 2\mu_m\left(\varepsilon_{ii}^{c} - \varepsilon_{ii}^{t}\right) + \lambda_m\sum_{j=1}^{3}\left(\varepsilon_{jj}^{c} - \varepsilon_{jj}^{t}\right) \end{aligned} \tag{7}$$

where $\mu = E/2(1+\nu)$ and $\lambda = 2\mu\nu/(1-2\nu)$ are the Lamé constants. Equations (6) and (7) form a system of six equations where $\varepsilon_{ii}^{c}$ and $\varepsilon_{ii}^{t}$ are the solutions. The stresses are calculated using Hooke's law.

Figure 10A shows the variation of the thermal residual stresses for the LS2 phase as a function of the crystallized volume fraction (*f*) considering a sphere in an LS2 glass matrix. All components are compressive, with the magnitude of each component being proportional to the difference with TEC of the glass matrix. All components also decrease with increasing *f*. The average residual stress is close to the $\sigma_{33}$ component (c-axis) and for low *f* is close to the stress predicted by Selsing's model. The effect of thermal expansion anisotropy is to induce higher compressive stresses along the lowest TEC (b-axis unit cell).

Figure 10B shows the calculated stresses considering the precipitate as an ellipsoid with an aspect ratio of 10. The long

**TABLE 8** Estimated composition of the residual glasses of EH and HH glass-ceramics, considering the crystal phases formed

| | EH (%mol) | HH (%mol) |
|---|---|---|
| $SiO_2$ | 69.04 | 71.29 |
| $Li_2O$ | 12.48 | 9.86 |
| $P_2O_5$ | 1.21 | 1.86 |
| $Sb_2O_3$ | 1.60 | 1.96 |
| $K_2O$ | 9.36 | 10.07 |
| MgO | 2.56 | — |
| $Al_2O_3$ | 2.87 | — |
| CaO | 0.53 | — |
| BaO | 0.35 | — |
| ZnO | — | 0.43 |
| $Na_2O$ | — | 4.53 |

**TABLE 9** Experimental strains measured using XRD along the unit cell directions and average stresses in the $Li_2Si_2O_5$ crystals for the different glass-ceramics. The numbers in brackets are the standard deviations corresponding to the last significant digit

| Sample | $\varepsilon_a$ (%) | $\varepsilon_b$ (%) | $\varepsilon_c$ (%) | $\bar{\sigma}_{exp}$ (MPa) |
|---|---|---|---|---|
| EL | −0.026 (5) | −0.148 (5) | 0.018 (3) | −102 (9) |
| EH | −0.001 (3) | −0.012 (3) | −0.005 (2) | −12 (8) |
| HL | 0.037 (2) | −0.031 (2) | −0.071 (2) | −43 (2) |
| HH | 0.007 (2) | −0.030 (2) | −0.052 (2) | −49 (2) |
| IPS e.max® CAD | 0.085 (6) | −0.064 (5) | −0.063 (5) | −28 (6) |
| IPS e.max® PRESS | 0.090 (6) | −0.065 (4) | −0.111 (9) | −43 (9) |

ellipsoid axis is aligned along the c-axis of the LS2 unit cell. The effect of the ellipsoid shape is to increase the compressive stress along the ellipsoid longest direction (c-axis) and to increase slightly the average residual stress in the crystal.

At first sight, those plots seem to be counter intuitive. Zero crystallized fraction, f ~ 0, in reality means a particular case of one extremely small crystal embedded in the glassy matrix. The magnitude of the calculated (compressive) stress in the crystals decreases with increasing f because the difference between the average TEC of the crystals and that of the glass matrix decreases. With increasing f, the average TEC of the composite tends to that of the crystals, hence the TEC difference tends to zero for f tending to 1. Obviously, the stress level in the residual glass matrix increases with increasing f.

Table 10 shows the average residual stresses at the LS2 crystals using Equations (6) and (7) for a single ellipsoidal LS2 precipitate embedded in a matrix with thermal expansion $\alpha_{gc.exp}$, with the advantage that $\alpha_{gc.exp}$ is measured experimentally. A note must be added to this calculation; a comparison between the X-ray diffractograms of Figure 5 used for residual stress determination and those used for the determination of the volume fraction of the phases listed in Table 3 (difractograms not shown) reveals differences in the relative intensities of the LS phase in some samples. Some samples were produced at different moments, but were submitted to the same heat treatments for residual stresses and phase quantification measurements. The EH sample used for residual stress determination shows the presence of the LS phase, whereas that used for phase quantification did not. Moreover, the LS phase was not present in the HH sample used for residual stress but was present in the HH sample used for volume fraction determination. It is known that in some conditions in stoichiometric LS2 glass, the LS phase nucleates before the LS2 phase. With further heat treatment, the LS phase disappears and the LS2 phase predominates.[47] We do not know exactly the sequence of nucleation and growth of each phase in our complex, multicomponent glasses. In our opinion, the observed differences in concentration of the LS phase are due to small differences in the temperature during heat treatments due to different furnaces, thermocouple calibration, etc., which, in some cases, favored the LS formation. This shows the difficulties in producing the desired microstructures in these complicated multicomponent GCs. Therefore, for the calculation of the residual stress in the LS2 phase, we assumed, as an approximation, that the residual glass fractions were the same in the samples used for residual stress and phase quantification. Then, the residual stresses were calculated in a sample with the composition as determined using data from Table 3 utilized for phase quantification and in a sample with composition given by the relative phase concentrations from Rietveld refinement of samples used for residual stress determination. The residual stresses for all samples were taken as the average of these two stresses and the values are shown in Table 10.The calculated values are compared with the average stress from XRD experiments in Table 10. The calculated residual stresses followed the same trend as the experimental stresses, eg, samples with the highest experimental residual stresses also show the highest calculated stresses. Several possible factors that could affect the experimental stresses are not taken into account in the model. One is elastic anisotropy. It is expected that the elastic constants of the orthorhombic LS2 unit cell will vary along the unit cell directions. Depending on the degree of variation, these might greatly affect the residual stresses. Another cause is due to the different crystallized phases. The main other phases are $Li_3PO_4$ and $Li_2SiO_3$, as reported in Table 3. This phase combination affects not only the elastic constants of the GCs, but also their thermal expansion. Usually, the TECs of our GCs are higher than the TEC of the LS2 phase and the residual glass, as demonstrated in Tables 6 and 7.

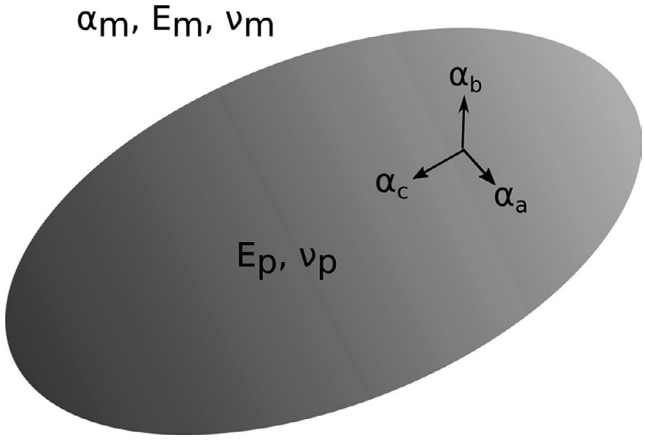


**FIGURE 9** Schematic representation of a lath-shaped LS2 precipitate as an ellipsoid in a glass matrix. The thermal expansion anisotropy of the ortorhombic LS2 phase is considered

Table 11 shows the experimental data for the higher crystallized volume fraction GCs. Sample EH showed the highest

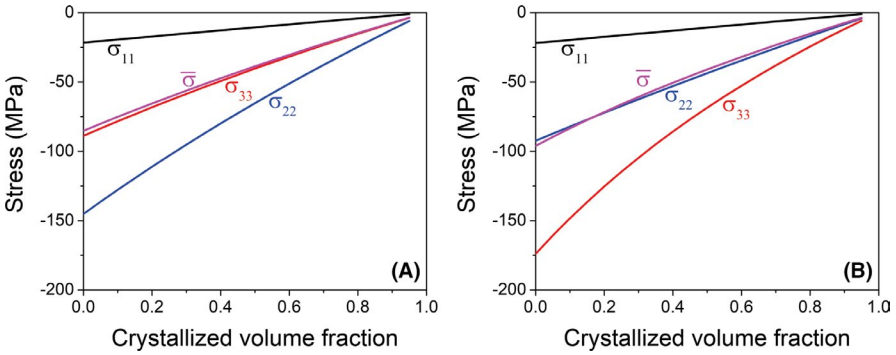


**FIGURE 10** Variation of the thermal residual stress components and average stress in the crystals with crystallized volume fraction (*f*) predicted using Equations (6) and (7) for a sphere (A), and an ellipsoid (c/a = 10) (B), considering the thermal expansion anisotropy of the LS2 phase

**TABLE 10** Comparison of the experimental (average) residual stresses, $\bar{\sigma}_{exp}$, at the LS2 crystals with the average stress, $\bar{\sigma}_{th}$, calculated using Equations (6) and (7) considering a single ellipsoid with 10:1 ratio in a matrix with TEC $\alpha_{gc.exp}$

| Sample | $\alpha_{gc.exp}$ ($10^{-6}$ K$^{-1}$) | *E* (GPa) | $\bar{\sigma}_{th}$ (MPa) | $\bar{\sigma}_{exp}$ (MPa) |
|---|---|---|---|---|
| EH | 10.4 | 98 | −27 | −12 ± 8 |
| HH | 12.3 | 107 | −110 | −49 ± 2 |
| CAD | 10.7 | 95 | −39 | −28 ± 6 |
| PRESS | 10.9 | 95 | −48 | −43 ± 9 |

Abbreviation: TEC, thermal expansion coefficient.

fracture toughness among the measured samples. Several factors influence fracture toughness in GCs. It was previously demonstrated that higher crystallized volume fraction and elastic modulus increase fracture toughness.[33] All samples have approximately the same crystalline volume fraction as the LS2 phase ($f_{LS2}$), varying from 33% to 38%. However, sample EH has the lowest *f* and E, indicating that these are not the most important factors determining its higher toughness.

Sample EH had the lowest compressive thermal residual stress in the LS2 crystals. However, the analysis of the effect of residual stresses is complicated in our samples due to the existence of different phases and crystallized volume fractions. Other samples presented different concentrations from 3% to 7% of $Li_3PO_4$, and 7% of the LS phase in sample HH. These phases have different thermal expansion anisotropies and shapes, which in turn will affect the residual stresses inside the GCs.

Taya et al have estimated the contribution of the residual stresses for the increase or decrease of the fracture toughness.[48] Their conclusion is that if the average residual stress in the *matrix* is compressive, any crack will be subjected to a closure stress at its tip, which will increase the fracture toughness. On the contrary, if the residual stress is tensile, there will be a decrease in the toughness. The change in toughness is a function of the magnitude of the residual stress and the distance between the precipitates. This model has been tested experimentally.[49,50] The toughness of glass samples with different concentrations of alumina was measured at room temperature and 500°C. At 500°C, the residual stresses were much smaller than at room temperature, as expected. However, there was no difference in fracture toughness with alumina concentration for these two temperatures, indicating that residual stresses may have no effect on fracture toughness.

We expected the best case of residual stresses (compressive or tensile) on fracture toughness would be for the lowest difference in the TECs between the crystals and glass matrix. The elastic energy in the matrix due to the residual stresses are proportional to the square of their magnitude. Since the residual stresses are directly proportional to the difference between the TECs of the crystals and the matrix, a smaller difference in the TECs will reduce the stored elastic energy available for the creation or propagation of cracks.

Compressive stresses in the precipitates (as is the case of this study) induce stresses in the glass matrix with the radial component in compression and the tangential components in tension.[21,44,51] For tensile residual stresses in the precipitate, the radial component is tensile, and the tangential components are compressive.[23,24]

Another important observation in the microstructure of the different GCs is the size of the LS2 crystals. Table 11 shows the smallest crystals, of approximately 1 μm in length, for the HH samples. The EH samples have long lath-shaped crystals, which are ~5 μm long. Recently, Senk demonstrated

**TABLE 11** Experimental data for the GCs with the highest crystallized volume fraction

| Sample | *E* (GPa) | $\bar{\alpha}_{LS2} - \alpha_{gc.exp}$ ($10^{-6}$ K$^{-1}$) | *f* (%) | $f_{LS2}$ (%) | LS2 crystal size (m) | $\bar{\sigma}_{exp}$ (MPa) | $K_{DTIC}$ (MPa·m$^{1/2}$) |
|---|---|---|---|---|---|---|---|
| EH | 98 | 0 | 41 | 34 ± 4 | 5 | −12 ± 8 | 2.2 |
| HH | 107 | −1.9 | 47 | 38 ± 5 | 1 | −49 ± 2 | 2.0 |

Abbreviation: GCs, glass-ceramics.

that the $K_{IC}$ of a stoichiometric LS2 GC increases with the crystal size.[52] It can be estimated that the toughness increases by 7% due to an increase of crystal size from 0.5 to 5 μm for a GC with $f = 55\%$, whereas in our work we observed an increase of 16%. Therefore, a higher crystal size may partially explain the increase in toughness of the EH sample by the R-curve mechanism. However, an excessively large crystal size would not be beneficial, as it may promote spontaneous microcracking under residual stress or under external mechanical load. Therefore, crystal sizes similar to those of the commercial IPS e.max® CAD and IPS e.max® PRESS GCs are desired.

Moreover, several other mechanisms, such as crack deflection, crack bowing and trapping, and crack bridging are effective in increasing the fracture toughness of GCs.[33] The lath shape of the LS2 crystals and their high-volume fraction help to produce an interlocking microstructure. This combination plus a large crystal size and a higher crystallized volume fraction are factors responsible for a GC with superior toughness.

In any case, we suggest that it could be revealing to extend this study by producing similar GCs having *tensile* residual stresses around the LS2 crystals. It could also be interesting to study similar GCs with significantly *higher level* of compressive stresses. Their toughness could then be compared with the current results for GCs having almost null or slightly compressive residual stresses (0-100 MPa).

## 5 | SUMMARY AND CONCLUSIONS

We designed and produced different GCs containing a major phase—micron-sized, lath-shaped LS2 crystals—and two other minor phases embedded within a residual glass having equal or larger TEC than the LS2 crystals. This design lead to different levels of compressive internal stresses, from almost null to slightly compressive. Different double-stage treatments for nucleation and crystal growth resulted in GC samples having from 22% to 48% crystallized volume fractions for both TEC cases. For comparative purposes, we also investigated two commercial dental GCs of the same family. We extended the Hsueh-Becher model (for hexagonal particles) to include the thermal expansion anisotropy of orthorhombic LS2 crystals and found that the average residual stresses in the LS2 precipitates in our GCs are highly anisotropic and are almost null or compressive.

The most important result of this research was that, within the levels of these residual stresses (0-100 MPa), we did not detect a significant effect in the fracture toughness. All in all, a highly crystallized volume fraction, relatively large crystal size (~5 μm), and the high elastic modulus of the LS2 crystals are responsible for the improvement of the fracture toughness of these GCs over their parent glasses. It could be revealing to extend this study for similar GCs having tensile residual stresses around the LS2 crystals. Such studies would be essential for the design of tough GCs.

## ACKNOWLEDGMENTS

The authors are grateful to FAPESP—Sao Paulo Research Foundation—(grant # 2013/07793-6) for generous funding and the Brazilian Synchrotron Light Laboratory (LNLS/CNPEM/Campinas) for supporting the research project XRD1-13534 and C-LABMU/UEPG for the use of the research facilities. We would also like to thank Dr. C. M. Lepienski for the instrumented indentation tests. We also thank CNPq (process number 142561/2010-0), Brazil, for granting a PhD fellowship to M. O. C. Villas Boas and CAPES, Brazil, for supporting PPGCEM-UFSCar.

## ORCID

*Mariana O. C. Villas-Boas* https://orcid.org/0000-0002-6083-8281

*Francisco C. Serbena* https://orcid.org/0000-0001-5293-628X

*Viviane O. Soares* https://orcid.org/0000-0002-0205-6118

*Edgar D. Zanotto* https://orcid.org/0000-0003-4931-4505

## REFERENCES

1. Deubener J, Allix M, Davis MJ, Duran A, Höche T, Honma T, et al. Updated definition of glass-ceramics. J Non-Cryst Solids. 2018;501:3–10.
2. Zanotto ED. A bright future for glass-ceramics. Am Ceram Sock Bull.? 2010; 89(8):19–27.
3. Davis MJ, Zanotto ED. Glass-ceramics and realization of the unobtainable: property combinations that push the envelope. MRS Bull. 2017; 42(3):195–9.
4. Martellato VR, Zanotto ED. Anisotropic residual stresses in partially crystallized $Li_2O$-$2SiO_2$ glass-ceramics. J Non-Cryst Solids. 1999; 247(1–3):79–86.
5. Fernandes HR, Tulyaganov DU, Goel A, Ribeiro MJ, Pascual MJ, Ferreira J. Effect of $Al_2O_3$ and $K_2O$ content on structure, properties and devitrification of glasses in the $Li_2O$-$SiO_2$ system. J Eur Ceram Soc. 2010;30(10):2017–30.
6. Wen G, Zheng X, Song L. Effects of $P_2O_5$ and sintering temperature on microstructure and mechanical properties of lithium disilicate glass-ceramics. Acta Mater. 2007;55(10):3583–91.
7. Tulyaganov DU, Agathopoulos S, Kansal I, Valério P, Ribeiro MJ, Ferreira J. Synthesis and properties of lithium disilicate glass-ceramics in the system $SiO_2$-$Al_2O_3$-$K_2O$-$Li_2O$. Ceram Int. 2009;35(8):3013–9.
8. Braun SE. Efeito do grau de cristalização nas propriedades mecânicas das vitrocerâmicas de dissilicato de lítio (Effect of crystallization degree on mechanical properties of lithium disilicate

glass-ceramics), M.Sc. dissertation (Graduate Program in Physics). Curitiba, Paraná, Brazil: Physics Department, Federal University of Paraná; 2008.
9. Apel E, Deubener J, Bernard A, Höland M, Müller R, Rheinberger V, et al. Phenomena and mechanisms of crack propagation in glass-ceramics. J Mech Behav Biomed Mater. 2008;1(4):313–25.
10. Zanotto ED, Leite M. The nucleation mechanism of lithium disilicate glass revisited. J Non-Cryst Solids. 1996;202(1–2):145–52.
11. Soares PC, Lepienski CM. Residual stress determination on lithium disilicate glass-ceramic by nanoindentation. J Non-Cryst Solids. 2004;348:139–43.
12. Zheng X, Wen G, Song L, Huang XX. Effects of $P_2O_5$ and heat treatment on crystallization and microstructure in lithium disilicate glass ceramics. Acta Mater. 2008;56(3):549–58.
13. Apel E, Hoen C, Rheinberger V, Höland W. Influence of $ZrO_2$ on the crystallization and properties of lithium disilicate glass-ceramics derived from a multi-component system. J Eur Ceram Soc. 2007;27(2–3):1571–7.
14. Fernandes HR, Tulyaganov DU, Ferreira J. The role of $P_2O_5$, $TiO_2$ and $ZrO_2$ as nucleating agents on microstructure and crystallization behaviour of lithium disilicate-based glass. J Mater Sci. 2013;48(2):765–73.
15. Ananyhanarayanan A, Kothiyal GP, Montagne L, Revel B. MAS-NMR investigations of the crystallization behaviour of lithium aluminum silicate (LAS) glasses containing $P_2O_5$ and $TiO_2$ nucleants. J Solid State Chem. 2010;183(6):1416–22.
16. IPS e.max Press [homepage on the internet]. No date. http://www.ivoclarvivadent.com/en/all/products/all-ceramics/ips-emax-technicians/ips-emax-press. Accessed April 4, 2019.
17. IPS e.max CAD [homepage on the internet]. No date. http://www.ivoclarvivadent.com/en/p/all/ips-emax-system-dentists/ips-emax-cad-chairside. Accessed April 4, 2019.
18. Camposilvan E, Leone R, Gremillard L, Sorrentino R, Zarone F, Ferrari M, et al. Aging resistance, mechanical properties and translucency of different yttria-stabilized zirconia ceramics for monolithic dental crown applications. Dent Mater. 2018;34(6):879–90.
19. Pedrosa AC. Sistemas cerâmicos metal free (Metal free ceramic systems) [homepage on the internet]. No date. http://www.iesposgraduacao.com.br/_downloads/pdf/artigo_alexandre.pdf. Accessed April 4, 2019.
20. César PF. Cerâmicas odontológicas (Dental ceramics) [homepage in the internet]. No date. Accessed April 4, 2019. Available from https://edisciplinas.usp.br/pluginfile.php/321282/mod_resource/content/0/2-Cer%C3%A2micas-2006-Texto-Colunas.pdf
21. Serbena FC, Soares VO, Peitl O, Pinto H, Muccilo R, Zanotto ED. Internal residual stresses in sintered and commercial low expansion $Li_2O$-$Al_2O_3$-$SiO_2$ glass-ceramics. J Am Ceram Soc. 2011;94(4):1206–14.
22. Mastelaro VR, Zanotto ED. Residual stresses in a soda-lime-silica glass-ceramic. J Non-Cryst Solids. 1996;194(3):297–304.
23. Serbena FC, Souza GP, Zanotto ED, Lumeau J, Glebova L, Glebov LB. Internal residual stresses in partially crystallized photo-thermo-refractive glass. J Am Ceram Soc. 2011;94(3):671–4.
24. Peitl O, Serbena FC, Mastelaro VR, Zanotto ED. Internal residual stress measurements in a bioactive glass-ceramic using Vickers indentation. J Am Ceram Soc. 2010;93(8):2359–68.
25. Pinto H, Ito L, Crovace M, Ferreira EB, Fauth F, Wroblewski T, et al. Surface and bulk residual stresses in $Li_2O.2SiO_2$ glass-ceramics. J Non-Cryst Solids. 2007;353(24–25):2307–17.
26. International glass database system—INTERGLAD, New glass forum in Japan [homepage on the internet]. No date. http://www.interglad.jp/. Accessed April 4, 2019.
27. SciGlass—Glass property information system, n.d. [homepage on the internet]. c2010 [updated 2011 May 16]. http://www.akosgmbh.de/sciglass/sciglass.htm. Accessed April 4, 2019.
28. Larson AC, Von Dreele RB. General structure analysis system (GSAS) (Report LAUR 86–748). Los Alamos, NM: Los Alamos Nat. Lab. Rep. LAUR; 2004.
29. Toby BH. EXPGUI, a graphical user interface for GSAS. J Appl Cryst. 2001;34:210–3.
30. Oliver WC, Pharr GM. An improved technique for determining hardness and elastic modulus using load and displacement sensing indentation experiments. J Mater Res. 1992;7(6):1564–83.
31. Niihara K. A fracture mechanics analysis of indentation-induced Palmqvist crack in ceramics. J Mater Sci Lett. 1983;2(5):221–3.
32. Quinn GD, Bradt RC. On the Vickers indentation fracture toughness test. J Am Ceram Soc. 2007;90(3):673–80.
33. Serbena FC, Mathias I, Foerster CE, Zanotto ED. Crystallization toughening of a model glass-ceramic. Acta Mater. 2015;86:216–28.
34. Evans AG. A method for evaluating the time-dependent failure characteristics of brittle materials and its application to polycrystalline alumina. J Mater Sci. 1972;7(10):1137–46.
35. Madjoubi MA, Hamidouche M, Bouaouadja N, Chevalier J, Fantozzi G. Experimental evaluation of the double torsion analysis on soda-lime glass. J Mater Sci. 2007;42(18):7872–81.
36. Shyam A, Lara-Curzio E. The double-torsion testing technique for determination of fracture toughness and slow crack growth behavior of materials: a review. J Mater Sci. 2006;41(13):4093–104.
37. Denry I, Holloway JA. Ceramics for dental applications: a review. Materials. 2010;3(1):351–68.
38. Willard A, Gabriel Chu TM. The science and application of IPS e.Max dental ceramic. Kaohsiung J Med Sci. 2018;34(4):238–42.
39. Höland W, Rheinberger V, Apel E, Ritzberger C, Eckert H, Mönster C. Mechanisms of nucleation and crystallization in high strength glass-ceramics. Phys Chem Glasses-Eur J Glass Sci Technol PART B. 2007;48(3):97–102.
40. Ritzberger C, Apel E, Höland W, Peschke A, Rheinberger VM. Properties and clinical application of three types of dental glass-ceramics and ceramics for CAD-CAM technologies. Materials. 2010;3(6):3700–13.
41. Richet P, Mysen BO, Andrault D. Melting and premelting of silicates: Raman spectroscopy and X-ray diffraction of $Li_2SiO_3$ and $Na_2SiO_3$. Phys Chem Miner. 1996;23(3):157–72.
42. Selsing J. Internal stresses in ceramics. J Am Ceram Soc. 1961;44(8):419–419.
43. Serbena FC, Zanotto ED. Internal residual stresses in glass-ceramics: a review. J Non-Cryst Solids. 2012;358(6–7):975–84.
44. Hsueh CH, Becher PF. Residual thermal stresses in ceramic composites. part I: with ellipsoidal inclusions. Mater Sci Eng A. 1996;212(1):22–8.
45. Eshelby JD, Peierls RE. The determination of the elastic field of an ellipsoidal inclusion, and related problems. Proc R Soc Math Phys Eng Sci. 1957;1226(241):376–96.
46. Sadd MH. Elasticity: theory, applications, and numerics, 3rd ed. Amsterdam, Boston: Elsevier/AP (Academic Press is an imprint of Elsevier); 2014.
47. Soares PC, Zanotto ED, Fokin VM, Jain H. TEM and XRD study of early crystallization of lithium disilicate glasses. J Non-Cryst Solids. 2003;331(1–3):217–27.

48. Taya M, Hayashi S, Kobayashi AS, Yoon HS. Toughening of a particulate-reinforced ceramic-matrix composite by thermal residual stress. J Am Ceram Soc. 1990;73(5):1382–91.
49. Kotoul M, Pokluda J, Sandera P, Dlouhy I, Chlup Z, Boccaccini AR. Toughening effects quantification in glass matrix composite reinforced by alumina platelets. Acta Mater. 2008;56(12):2908–18.
50. Todd RI, Boccaccini AR, Sinclair R, Yallee RB, Young RJ. Thermal residual stresses and their toughening effect in $Al_2O_3$ platelet reinforced glass. Acta Mater. 1999;47(11):3233–40.
51. Peitl O, Zanotto ED, Serbena FC, Hench LL. Compositional and microstructural design of highly bioactive $P_2O_5$–$Na_2O$–CaO–$SiO_2$ glass-ceramics. Acta Biomater. 2012;8(1):321–32.
52. Senk MV. Efeito da fração cristalina e tamanho de cristal na resistência mecânica e tenacidade à fratura da vitrocerâmica dissilicato de lítio. (Effect of crystalline fraction and crystal size in strength and fracture toughness of lithium disilicate glass-ceramics). M.Sc. dissertation (Programa de Pós-Graduação em Ciências). Paraná, Brazil: Physics Department, State University of Ponta Grossa; 2017.

**How to cite this article:** Villas-Boas MOC, Serbena FC, Soares VO, Mathias I, Zanotto ED. Residual stress effect on the fracture toughness of lithium disilicate glass-ceramics. *J Am Ceram Soc*. 2019;00:1–15. https://doi.org/10.1111/jace.16664